

# Effect of X-ray mirror figure error on the focus profile – comparison of measurements with physical and geometric optics simulations

David Laundry and Kawal Sawhney

Diamond Light Source, Harwell Science and Innovation Campus, Didcot, Oxon. OX11 0DE.  
UK

## ABSTRACT

Mirrors operating at grazing angles utilising total external reflection are commonly used for focusing X-ray at synchrotron radiation sources. Figure error on the mirror causes distortion of the focus profile. We have modeled a well characterized test mirror which has three different modifications of the elliptical figure laid down in parallel lanes running the length of the mirror. The focusing of the mirror was simulated using geometric optics (ray tracing) and physical optics (wave propagation). The mirror was then tested with X-rays on a beamline at a synchrotron radiation facility. The comparison between the two simulation methods and the measured data elucidates the origins of structures on the intensity profile of the focused beam and demonstrate that for quantitative agreement between simulation and experiment, interference and diffraction effects must be modeled.

**Keywords:** Synchrotron radiation, modeling, geometric optics, physical optics, X-ray mirror, focusing

## 1. INTRODUCTION

Mirrors operating at grazing angles utilising total external reflection are commonly used for focusing X-ray at synchrotron radiation sources. A typical arrangement is a Kirkpatrick-Baez (KB) pair<sup>1</sup> which is shown schematically in Fig. 1. The KB arrangement separates the horizontal from the vertical focusing which gives greater flexibility in design and alignment compared to schemes such as using ellipsoidal or toroidal mirrors in which the horizontal and vertical focusing is achieved by a single mirror. With the two mirrors, the horizontal and the vertical demagnification ratio and the numerical apertures can be optimized in design. Mirror alignment is simplified as the decoupling between horizontal and vertical directions allows independent optimisation of the horizontal and the vertical focus using the respective mirror pitch angles. The elliptical surface profile of each mirror is determined solely by the distance from the source to the mirror centre ( $P$ ), the distance from the mirror centre to the focal plane ( $Q$ ) and the glancing angle of incidence of the X-rays at the mirror centre ( $\theta$ ) and the magnification ratio is given by  $P/Q$ . KB mirrors are frequently employed in a highly demagnifying geometry  $P \gg Q$  to give focused beam sizes of less than 100 nm for microprobe type experiments. Elliptical mirrors also have the advantage that it is generally easier to manufacture surfaces that are profiled in a single direction only and therefore to obtain lower figure errors.

Simulations play a large role in the design and optimisation of X-ray beamlines. Geometrical optics in the form of ray tracing has traditionally been used to model X-rays as often wave diffraction and interference effects are masked by the size of the synchrotron radiation source. With the progress towards lower emittance sources providing high transverse coherent X-rays, wave propagation techniques are now more commonly used.<sup>2,3</sup> Simulations are particularly valuable for beamline design for predicting the X-ray intensity distribution at a sample position located at or near to a focal plane. It is at this position that the observed beam size may be larger than expected from the source size and the mirror slope error contribution due to diffraction. Diffraction is a consequence of the wave properties of the radiation and is therefore not predicted by geometric optics simulations.

---

Further author information: Send correspondence to DL, E-mail: david.laundry@diamond.ac.uk

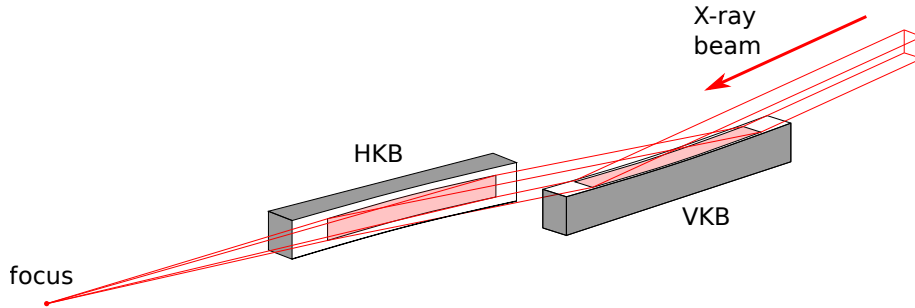


Figure 1. Two dimensional focusing of X-rays by a Kirkpatrick-Baez mirror pair consisting of a vertical focusing elliptical mirror (VKB) and a horizontally focusing elliptical mirror (HKB). The HKB is placed after the VKB in order to achieve a larger demagnification factor. The glancing angle of incidence is typically of order 3 mrad.

The ray tracing method tracks individual photons through the optical system. The photon starting position and directions are chosen at random using the known properties of the source. The coordinates are then traced through the system to the final detection plane and the intensity on this plane is given by the photon number density on this plane. Physical optics propagates the photon field amplitude using the Fresnel-Kirchhoff equation (Born and Wolf<sup>4</sup>) and the final intensity is given by the squared magnitude of the field amplitude. We have modeled a test mirror using geometrical optics and physical optics simulations and then made measurements on the mirror using the Test Beamline at Diamond Light Source.<sup>5</sup>

## 2. GEOMETRIC OPTICS SIMULATION

The test mirror was specified as part of a project to provide variable beam sizes for a macro-molecular beamline (Trincao et al<sup>6</sup>). Variable size focused X-ray beam can be achieved by various method – changing the surface profile of a bimorph mirror in order to change the mirror focal length (Alianelli et al, 2016<sup>7</sup>), using a combination of variable focus mirrors or compound refractive lenses to achieve a zoom configuration (Matsuyama et al, 2016,<sup>8</sup>

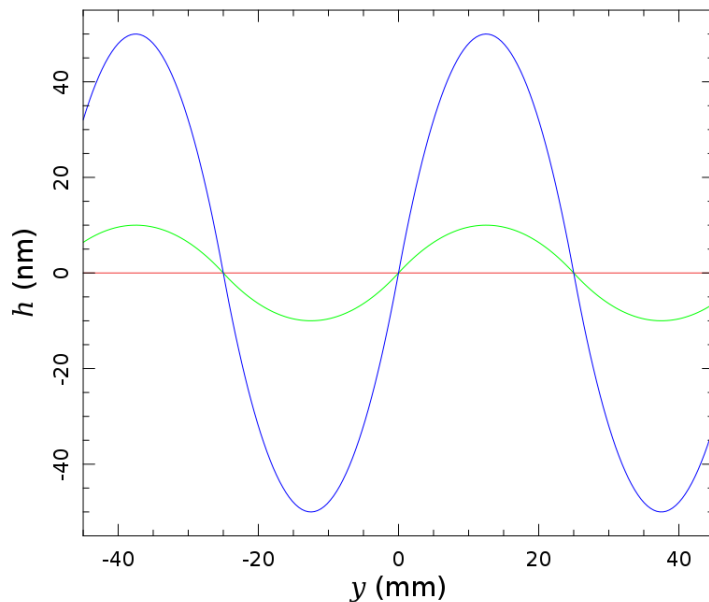


Figure 2. surface figure added to the basic elliptical profile for the three lane test mirror, red – lane 1 (zero), green – lane 2 20 nm peak-peak, blue lane 3 100 nm peak-peak. Each of the four sections of lane 2 and 3 is a parabolic arc

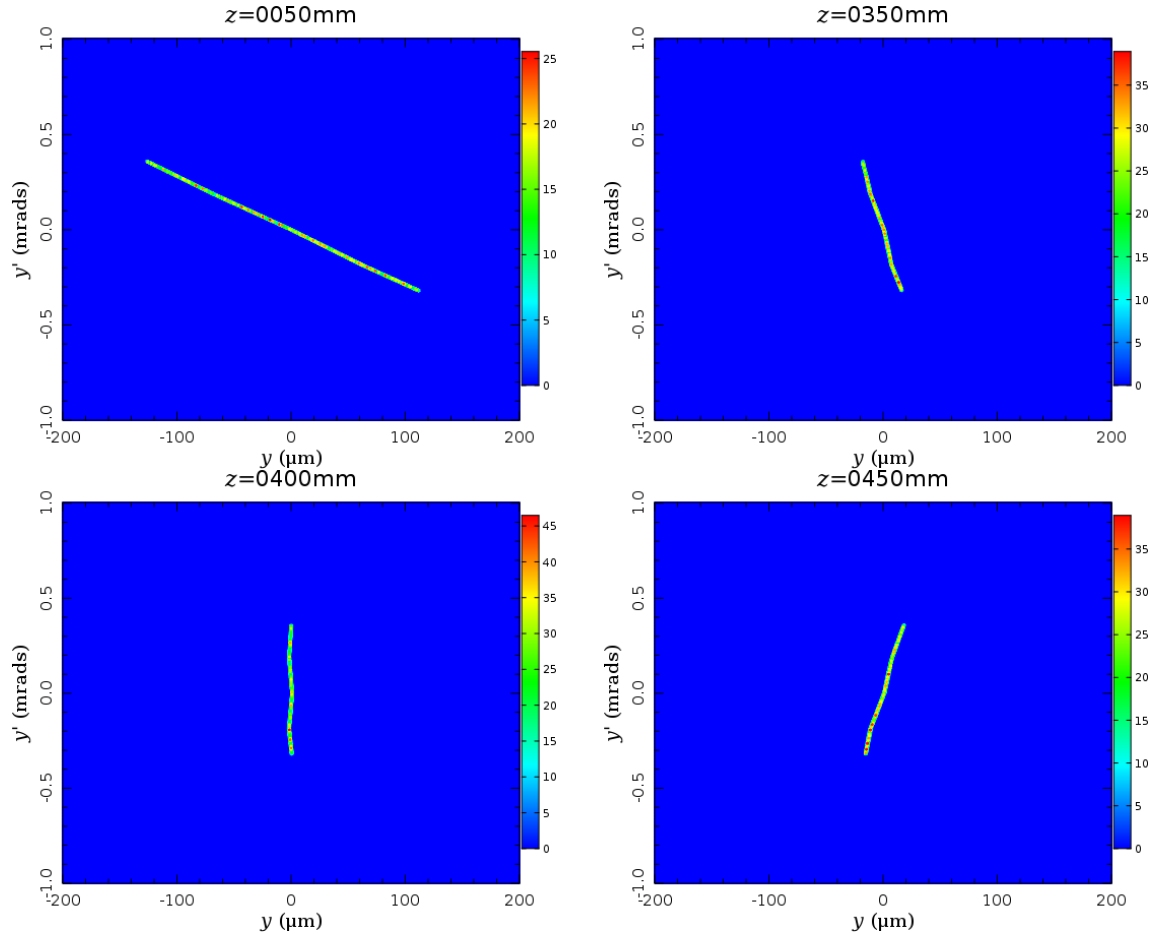


Figure 3. Vertical phase space ( $y, y'$ ) for the ray tracing calculation. The mirror has figure error given by lane 2 in Fig 2. Top left – 50 mm after the mirror, top right – 350 mm after the mirror, bottom left – 400 mm (focal plane), bottom right – 450 mm after the mirror.

Evans et al, 2007,<sup>9</sup> Schneider et al 2012<sup>10</sup>), using slits to change the size of a secondary source (Fischetti et al 2013<sup>11</sup>), spatially modulating the surface height of a focusing mirror (Laundy et al<sup>12,13</sup>) or using a refractive optical element to modulate the phase of the X-ray wavefront (Laundy et al, 2017<sup>14</sup>). This mirror was a prototype mirror specified with spatially modulated surface profile in order to achieve the required beam size at the sample. The prototype mirror was designed with three parallel lanes running the length of the mirror. The first lane had an elliptical figure in order to provide the smallest beam size of order  $1 \mu\text{m}$  at the focal plane. The second lane had a height modulation added to the basic elliptical figure designed to broaden the beam to  $2 \mu\text{m}$  at the focal plane and the third lane had an added height modulation designed to produce a  $10 \mu\text{m}$  beam at the focal plane. In order to obtain a top-hat like profile the addition height modulations were composed of parabolic arcs as shown in Fig. 2. By translating the mirror sideways, the X-ray beam can be moved to another lane to change the focused beam size. This test mirror also provides a convenient way of investigating the effect of figure error on measurements and simulations. The test mirror was manufactured to an elliptical profile with glancing angle of incidence of 3 mrad and source distance  $P = 45 \text{ m}$  and focus distance  $Q = 0.4 \text{ m}$ . The mirror was mounted to deflect the beam and focus vertically.

In the ray tracing simulations, the source was modeled as a dipole source with vertical rms dimension  $\sigma_y = 20 \mu\text{m}$ . The energy selected was 15 keV but as ray tracing does not model interference and diffraction effects, the energy selected has little effect on the results. The test mirror lane 1 was modeled as an ellipse and with the surface profiles in lane 2 and 3 added. The mirror focusing may be usefully visualized as a distribution  $\phi(y, y')$  in 2 dimensional phase space consisting of ray position variable  $y$  and ray angular variable  $y'$  as is shown

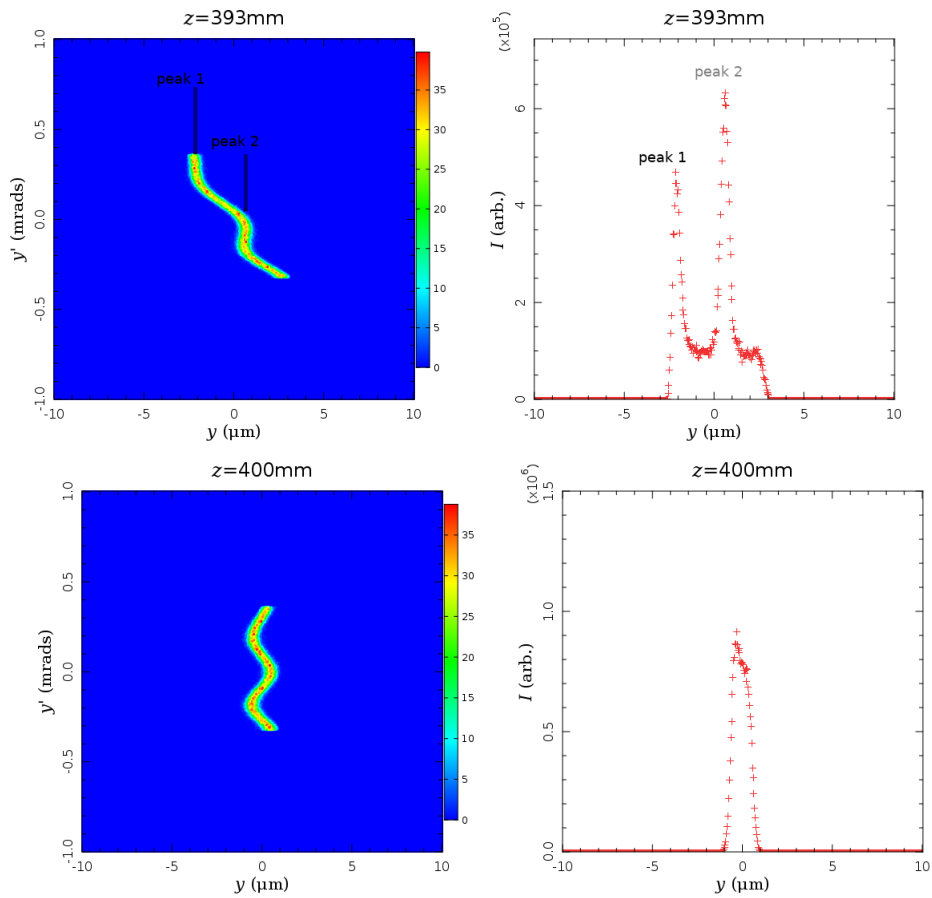


Figure 4. Vertical phase space  $(y, y')$  (left) and beam profile (right) for the ray tracing calculation. The mirror has figure error given by a sin wave. The two peaks occur in the intensity profile when  $dy'/dy$  becomes infinite i.e. at a point  $y_1$  where the locus of points marking the peak in phase space becomes vertical.  $z$  is the distance from the centre of the mirror with  $z = 400\text{mm}$  being the position of the mirror focal plane

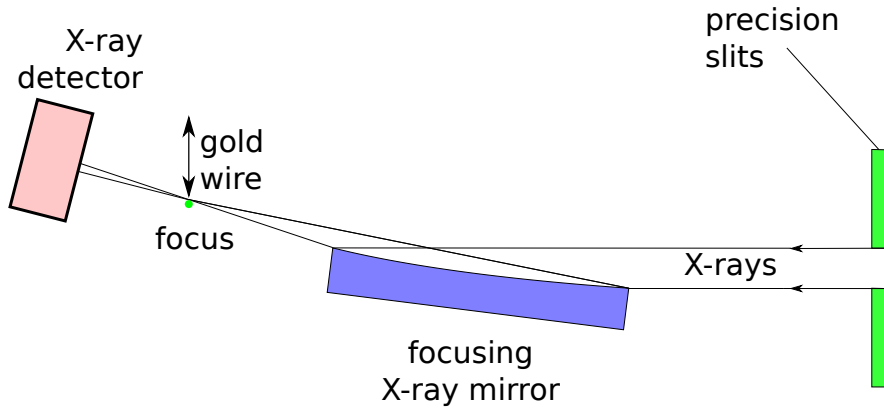


Figure 5. schematic diagram of the layout of the experiment on the Diamond Test Beamline

in Fig. 3. For lane 1, the rays are uniformly distributed along a narrow straight line which lies at an angle  $dy'/dy = 1/(Q - z)$  where  $z$  is the distance from the mirror. At the focal plane ( $z = Q$ ), the line is vertical and the beam size, the spread in  $y$  values, is at a minimum. For lane 2 and 3, the mirror surface modulation introduces a small perturbation along the  $y'$  direction for each ray. This perturbation when projected to the focal plane, appears as a displacement along the  $y$  direction. The beam intensity is calculated by integrating the phase space distribution along  $y'$  and results in an increase in the size of focal distribution.

$$I(y) = \int \phi(y, y') dy' \quad (1)$$

The intensity distribution is therefore a projection of a locust in phase space onto the  $y$  axis. Singularities occur when the gradient of the line becomes infinite as is demonstrated in Fig. 4. The strongest singularity occurs when this coincides with a point of inflection (i.e. zero curvature). At the focal plane any structures are obscured by the demagnified source contribution. The explanation for the peaks in the X-ray intensity distribution is essentially the same as the explanation of caustic structures from visible light optics in which reflection from a curved surface gives rise to a line of singularities however due to the decoupling of the horizontal and the vertical focusing in this case, these structures occur only in a Cartesian single dimension. The presence of these diffraction like structures at positions away from the focal plane of elliptical X-ray mirrors with figure error has been recognized (Sutter et al 2014<sup>15</sup>, Nicolas et al 2013<sup>16</sup>).

### 3. PHYSICAL OPTICS SIMULATIONS

Wavefront propagation was done using synchrotron radiation workshop (SRW)<sup>2</sup> and also using custom one dimensional propagation code. The system was modeled with the same parameters as used in the ray tracing calculation. The field amplitude was propagated across the mirror surface lying at low angle to the optical axis using analytic projection of the wavefront from a nominal plane before the mirror to a plane following the mirror, The field amplitude was propagated through free space from the source to the mirror and then from the mirror to the focal plane using the Fresnel-Kirchoff equation.

### 4. EXPERIMENTAL MEASUREMENTS

The mirror was mounted on the Diamond Test Beamline as shown schematically in Fig. 5. The X-ray energy was selected by a double crystal silicon 111 monochromator. The beam cross section was selected by slits to fully illuminate the mirror surface and a piezo tilt stage allowed the mirror angle to be optimized. At the focal plane, a  $50 \mu\text{m}$  diameter horizontally mounted gold wire was scanned through the beam on a piezo translation stage with an X-ray point detector mounted behind and the beam intensity profile was measured by taking the difference in measured intensity as the wire was stepped. Measurements were made using mirror lane 1 adjusting the mirror tilt angle  $\theta$  to get the narrowest focus profile and then the mirror was translated to lane 2 and 3 and the focal profile remeasured.

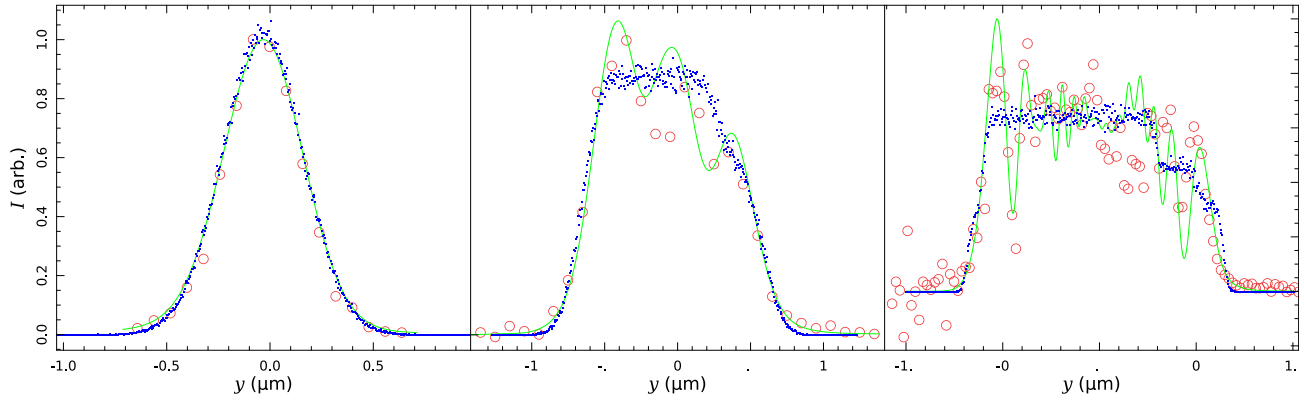


Figure 6. The X-ray beam profile at the focal plane – comparison of the experimental measurement with simulations. Left plot – mirror lane 1 (no figure modification of the mirror elliptical shape), middle plot – mirror lane 2 (20 nm peak to peak modification), right plot – mirror lane 3 (100 nm peak to peak modification). Red circles are the experimental measured X-ray intensity, blue dots is the simulated intensity by ray tracing and the green lines is the simulated intensity by wave propagation

Fig.6 shows the data obtained at a single energy (15 keV) for the three mirror lanes. Fig.7 shows the data for lane 3 at three different X-ray energies.

## 5. CONCLUSIONS

For mirror lane 1 with the unmodified elliptical surface, both ray tracing and wave propagation agree well with the experimental data shown in Fig. 6. This is not surprising as the beam profile is mainly determined by the profile of the demagnified X-ray source and the data could equally well be fitted by a Gaussian distribution of rms width  $\sigma = (Q/P)\sigma_y$  where  $\sigma_y$  is the electron beam source rms size and  $P$  and  $Q$  are the distances from source to mirror and from mirror to focus respectively. On the Test Beamline at Diamond, the source size is relatively large, however on undulator beamlines with smaller source size, the effects of residual figure error and diffraction broadening on the focal profile should be visible. For mirror lane 2 and lane 3 also shown in Fig. 6, the ray tracing predicts a profile with a flat top. The drop in intensity on the right side of the profiles for lane 2 and 3 is caused by the truncation of the figure modification in Fig. 2 at  $\pm 45$  mm thereby removing a section of the mirror that would have contributed to the positive edge of the focal profile. The experimental measurement shows significant structures which are reproduced in the wavefront simulations. These structures are caused by interference from different sections of the wavefront which overlap at the focal plane. In 2d phase space  $(y, y')$ , this corresponds

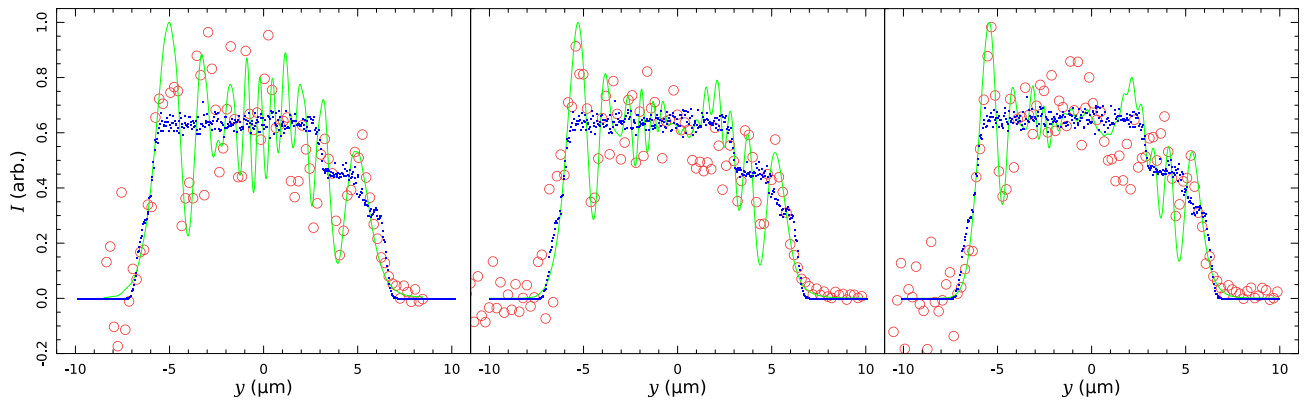


Figure 7. The X-ray beam profile at the focal plane – comparison of the experimental measurement for lane 3. Left plot – X-ray energy 10 keV, middle plot – X-ray energy 15 keV, right plot – X-ray energy 20 keV. Red circles are the experimentally measured X-ray intensities, blue dots show the simulated intensity obtained by ray tracing and the green lines show the simulated intensity obtained by wave propagation

to the integral in Eq. 1 crossing the locust of points at two or more positions. The ray tracing, however, doesn't model the interference, and therefore the intensity structures predicted by the wave propagation and observed in the measurement are not seen by the ray tracing. This is further illustrated in Fig. 7 which shows the measured and calculated focused beam profile for lane 3 for three different X-ray energies. The X-ray path length ( $d$ ) in the Fresnel-Kirchoff Equation is independent of X-ray energy but the phase factor  $\exp[i2\pi d/\lambda]$  which determines interference between different waves does depend on X-ray energy through the X-ray wavelength  $\lambda$ . At higher X-ray energy, smaller  $\lambda$ , the phase term is more rapidly varying and gives rise to shorter period fringes at the focus. This is apparent in the measurement and is also correctly modeled by the wave propagation calculation.

The measurements are highly demanding of mechanical stability of the mirror and it is quite likely that micro radian scale drifts of the mirror pitch angle  $\theta$  over the time scale of the measurement are affecting the result. We however conclude that for this optical system, ray tracing predicts in a qualitative way, the profiles of the focused beam but fails to model effects caused by coherence of the wavefront. For some applications, this may be adequate but for quantitative prediction of the intensity distribution, wave interference effects must also be modeled.

## 6. ACKNOWLEDGMENTS

This work was carried out with the support of Diamond Light Source.

## REFERENCES

1. P. Kirkpatrick and A. V. Baez, "Formation of optical images by X-rays.," *Journal of the Optical Society of America* **38**, pp. 766–774, sep 1948.
2. O. Chubar, "Precise computation of electron-beam radiation in nonuniform magnetic fields as a tool for beam diagnostics," *Review of Scientific Instruments* **66**(2), p. 1872, 1995.
3. D. Laundry, J. P. Sutter, U. H. Wagner, C. Rau, C. a. Thomas, K. J. S. Sawhney, and O. Chubar, "Parallel simulations of partially coherent wavefront propagation from a finite emittance electron beam," *Journal of Physics: Conference Series* **425**, p. 162002, mar 2013.
4. M. Born and E. Wolf, *Principles of Optics*, vol. 10, Cambridge University Press, 1999.
5. K. J. S. Sawhney, I. P. Dolbnya, M. K. Tiwari, L. Alianelli, S. M. Scott, G. M. Preece, U. K. Pedersen, R. D. Walton, R. Garrett, I. Gentle, K. Nugent, and S. Wilkins, "A Test Beamline on Diamond Light Source," **1234**(1), pp. 387–390, AIP Publishing, 2010.
6. J. Trincao, A. Warren, P. Aller, G. Duller, K. Wilkinson, A. Stallwood, D. Laundry, L. Allianelli, K. Sawhney, G. Rehm, and G. Evans, "VMXm: a new sub-micron beamline for macromolecular crystallography at Diamond Light Source," *Acta Crystallographica Section A Foundations and Advances* **71**, pp. s191–s191, aug 2015.
7. L. Alianelli, D. Laundry, S. Alcock, J. Sutter, and K. Sawhney, "Development of Hard X-ray Focusing Optics at Diamond Light Source," *Synchrotron Radiation News* **29**, pp. 3–9, jul 2016.
8. S. Matsuyama, H. Nakamori, T. Goto, T. Kimura, K. P. Khakurel, Y. Kohmura, Y. Sano, M. Yabashi, T. Ishikawa, Y. Nishino, and K. Yamauchi, "Nearly diffraction-limited X-ray focusing with variable-numerical-aperture focusing optical system based on four deformable mirrors," *Scientific Reports* **6**, p. 24801, apr 2016.
9. G. Evans, L. Alianelli, M. Burt, A. Wagner, and K. J. S. Sawhney, "Diamond Beamline 124: A Flexible Instrument for Macromolecular Micro-crystallography," in *AIP Conference Proceedings*, **879**(1), pp. 836–839, AIP, 2007.
10. D. K. Schneider, L. E. Berman, O. Chubar, W. A. Hendrickson, S. L. Hulbert, M. Lucas, R. M. Sweet, and L. Yang, "Three Biomedical Beamlines at NSLS-II for Macromolecular Crystallography and Small-Angle Scattering," *Journal of Physics: Conference Series* **425**, p. 012003, mar 2013.
11. R. F. Fischetti, D. Yoder, S. Xu, O. Makarov, C. Ogata, and J. L. Smith, "Predicted optical performance of the GM/CA@APS micro-focus beamline," *Journal of Physics: Conference Series* **425**, p. 012006, mar 2013.
12. D. Laundry, L. Alianelli, J. Sutter, G. Evans, and K. Sawhney, "Surface profiling of X-ray mirrors for shaping focused beams," *Optics Express* **23**, p. 1576, jan 2015.
13. D. Laundry, K. Sawhney, I. Nistea, S. G. Alcock, I. Pape, J. Sutter, L. Alianelli, and G. Evans, "Development of a multi-lane X-ray mirror providing variable beam sizes," *Review of Scientific Instruments* **87**, p. 051802, may 2016.
14. D. Laundry, K. Sawhney, and V. Dhamgaye, "Using refractive optics to broaden the focus of an X-ray mirror," *Journal of Synchrotron Radiation* **24**(4), pp. 744–749, 2017.
15. J. P. Sutter, S. G. Alcock, F. Rust, H. Wang, and K. Sawhney, "Structure in defocused beams of x-ray mirrors: causes and possible solutions," p. 92080G, International Society for Optics and Photonics, sep 2014.
16. J. Nicolas and G. García, "Modulation of intensity in defocused beams," in *Proceedings of SPIE, Advances in X-ray/EUV Optics and Components VIII*, A. Khounsary, S. Goto, and C. Morawe, eds., **8848**, p. 884810, sep 2013.